THIRTEENTH EUROPEAN ROTORCRAFT FORUM

2.19
Paper No. 66

NEW AERODYNAMIC ROTOR BLADE DESIGN AT MBB

G. Polz, D. Schimke

Messerschmitt-Bölkow-Blohm GmbH
Munich, Germany

September 8-11, 1987
Arles, France

ASSOCIATION AERONAUTIQUE ET ASTRONAUTIQUE DE FRANCE

NEW AERODYNAMIC ROTOR BLADE DESIGN AT MBB

G. Polz, D. Schimke

Messerschmitt-Bölkow-Blohm GmbH
Munich, Germany

Abstract

For the next generation of MBB helicopters a new rotor blade with an advanced aerodynamic and structural design was developed at MBB.

Basic requirements of the blade layout were a significant reduction of power consumption and a shift of transonic operational boundaries to higher Mach numbers, as compared to the standard BO105 rotor blade, combined with good thrust capability and handling qualities. For achieving these goals new advanced airfoils and specific blade planforms and tip shapes were integrated in the design.

A model rotor of 4 m diameter was built and tested in a wind tunnel up to speeds of 300 km/hr, verifying the predicted rotor characteristics for the whole range of speeds and blade loadings.

With a full scale rotor, suitable for the BO105, model rotor test results were verified in whirl tower and flight tests. A considerable reduction in reqired power as compared to the BO105 standard rotor, was achieved.

Advancing blade tip Mach numbers of .95 were obtained during the flight tests without severe degradation of handling qualities. Also vibration and noise were significantly reduced as compared to the standard BO105 rotor system.

List of Symbols and Abbreviations

c	m	blade chord
C_D	-	airfoil drag coefficient
C_L	-	airfoil lift coefficient
C_M	-	airfoil pitching moment coefficient
C_T	-	rotor thrust coefficient
C_Q	-	rotor power coefficient
g	m/s^2	gravity factor
m	kg	gross mass
M	-	Mach number
n_z	g	load factor
OAT	deg C	outside air temperature
R	m	rotor radius

V	km/hr	flight speed
V_H	km/hr	maximum crusing speed
z	-	number of blades
m	-	advance ratio (= V/L R)
L	1/s	rotor angular velocity
p	kg/m^3	air density
s	-	rotor disk area solidity

1. Introduction

The improvement of helicopter aerodynamics in order to increase cruise speed and payload and to decrease fuel consumption is a general target for the helicopter industry. One of the most essential tasks with chances for success is the improvement of the rotor performance, as the use of modern composite materials allows a rotor blade design with nearly arbitrary shape for optimization of blade aerodynamics.

Aerodynamic studies on advanced rotor blade design were started at MBB in 1972. In the following years several versions of the AGB (Advanced Geometry Blade, s. Fig. 1) have been tested on the BO105 HGH, a high speed test version of the BO105, up to speeds of 400 km/hr /1/. The latest version was the AGB IV, which made its first flight in 1977. It showed a remarkable reduction in power consumption combined with good control characteristics and low vibration levels /2/.

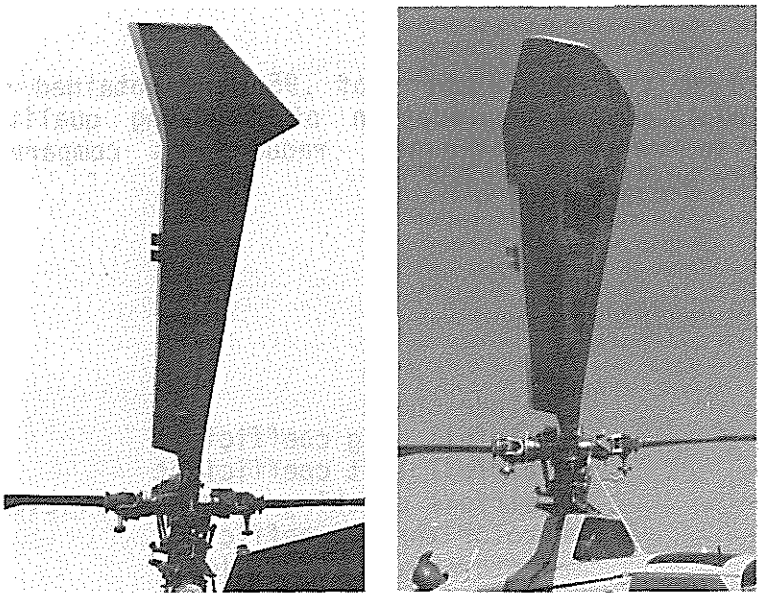

AGB III AGB IV

Fig. 1: Advanced geometry blades (experimental versions)

At the beginning of the 80's first studies on a new rotor concept were conducted, combining the advantages of new airfoils, optimized blade geometry and modern structural design.

2. Development of new Airfoils

In 1981 a cooperation was started between MBB and DFVLR for developing advanced helicopter rotor airfoils. Requirements based on the aerodynamic characteristics of the best existing airfoils and the operational conditions of helicopter rotors, up to flight speeds of 280 km/hr, were specified in terms of maximum lift at low Mach numbers, lift-to-drag ratio at medium Mach numbers, transonic drag at near zero lift, and maximum allowable pitching moment (Table 1).

design objective	inner airfoil	tip airfoil
thickness	12%	9%
drag divergence ($c_D = 0.02$)	$M > 0.8$ at $c_L = 0/0.2$	$M > 0.84$ at $c_L = -0.2/0$
drag at $M = 0.6$, $c_L = 0.7$	$c_D \leq 0.01$	$c_D \leq 0.01$
maximum lift at $M = 0.3$ $M = 0.4$ $M = 0.5$	$c_{Lmax} = 1.5$ 1.4 1.3	$c_{Lmax} = 1.3$ 1.2
pitching moment below stall inception	$\lvert c_M \rvert \leq 0.01$	$\lvert c_M \rvert \leq 0.01$

Table 1: Blade airfoil design objectives

Two airfoils, one for the blade tip and one for the inner blade region, designated DM-H1 Tb and DM-H2 Tb, were designed and investigated in the transonic wind tunnel of the DFVLR /3/. These airfoils fulfilled almost completely the requirements with regard to aerodynamic performance and moment behavior. The experience gained during the design process of the new airfoils offered the possibility to improve or to change some of their characteristics in view of a higher degree of adaption to rotor requirements. In order to realize the possible improvements, the airfoils were modified, leading to the new versions DM-H3 Tb for the blade tip and DM-H4 Tb for the inner blade parts /4/. Wind tunnel tests showed, that all requirements have been fulfilled (Fig. 2).

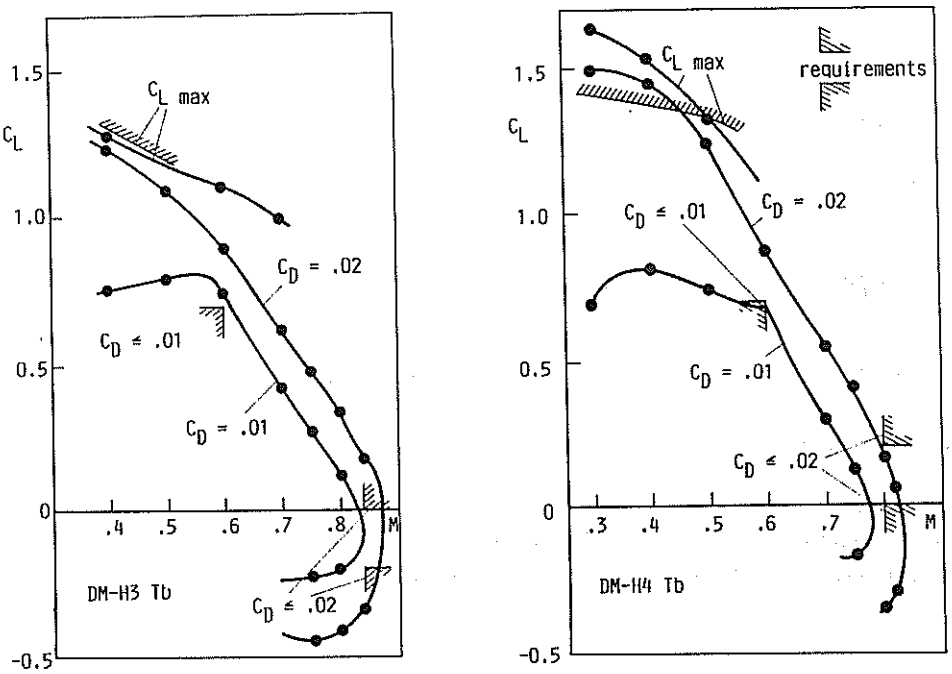

Fig. 2: Aerodynamic performance of the rotor blade airfoils DM-H3 Tb and DM-H4 Tb

The favourable aerodynamic characteristics of both airfoils are demonstrated in Fig. 3, through comparison with other good airfoil families, in terms of maximum lift versus drag divergence Mach number.

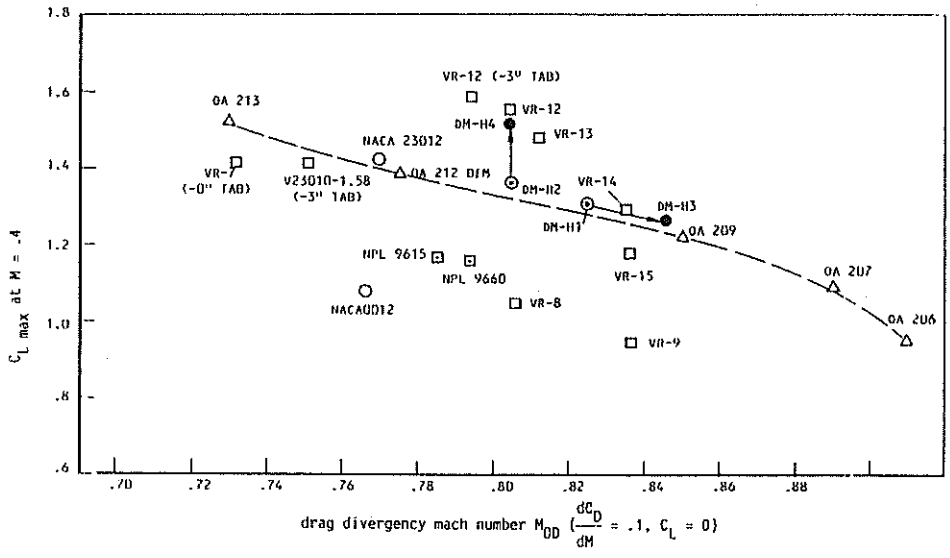

Fig. 3: Maximum lift coefficient vs. drag divergence Mach number of several rotor blade airfoils

For the DM-H3 Tb the Mach tuck, i.e. the begin of rapid change of pitching moment versus Mach number at constant lift /7/, has been shifted forward to higher Mach numbers and thus to higher flight speeds by an amount of approximately 50 km/hr, compared to the NACA 23012 (Fig. 4).

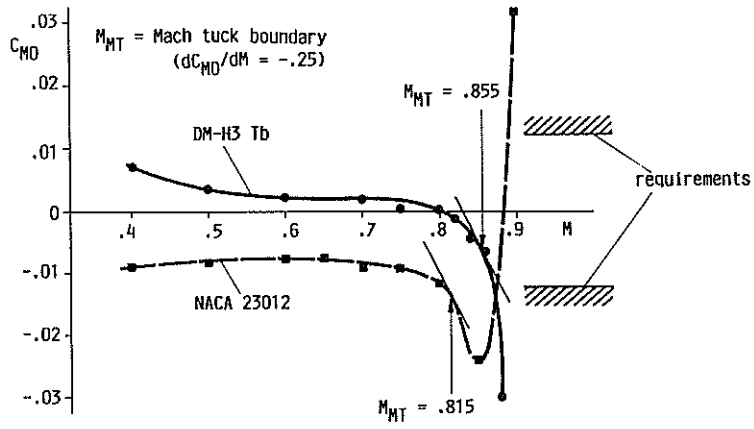

Fig. 4: Zero lift pitching moment behavior of the DM-H3 Tb airfoil compared to the NACA 23012.

To get more confidence in the measured aerodynamic characteristics of the new airfoils, the DM-H4 Tb has been tested additionally in the ONERA S3 wind tunnel at Modane, showing very good agreement with the DFVLR test results. Another transonic test of the DM-H3 Tb has been conducted at the Universität der Bundeswehr München at Mach numbers up to 1.1. These tests were possible due to accurate control of the boundary suction on the wind tunnel walls.

Typical pressure distributions are shown in Fig. 5 for both DM-airfoils. For the DM-H3 Tb a low level of the suction peaks on the upper and lower surface was desired to minimize the transonic wave drag. At high Mach number and low lift coefficient on the upper surface a laminar flow up to 30% chord length could be achieved. The DM-H4 Tb, designed for high maximum lift at low Mach numbers, is characterized by a moderate suction peak (max. Mach number ≈ 1.4) on the upper surface, which prevents from premature flow seapration and high wave drag.

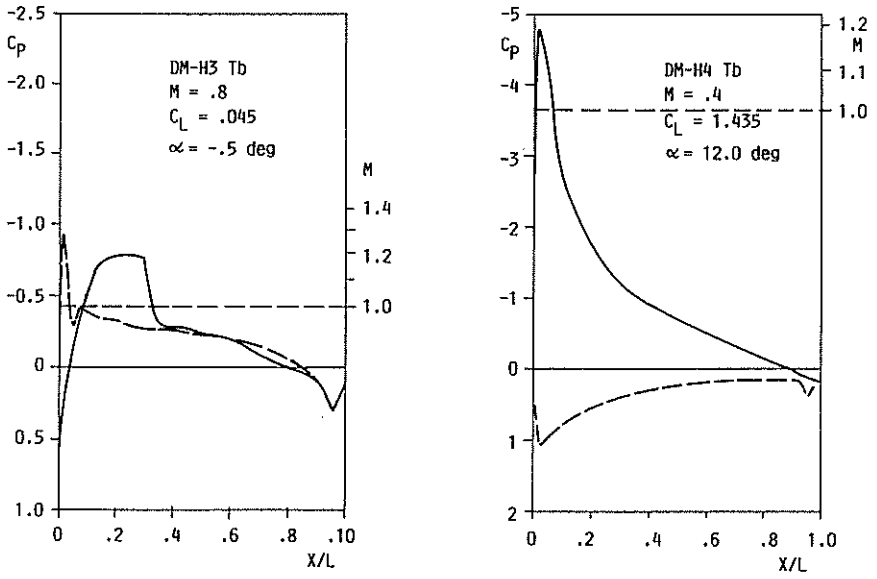

Fig. 5: Typical pressure distributions of the DM airfoils

3. Blade Planform and Tip Shape

Improvements in power consumption and general aerodynamic behavior can be obtained by specific design of blade planform and tip geometry, as the use of modern composite material allows nearly arbitrary shape of the blades.

The dominant contribution of the outer blade parts to the rotor power consumption, which can be deducted from the formula

$$P = Z \cdot \frac{\rho}{2} \cdot \Omega^3 \cdot C_D \int_0^R c(r) \cdot r^3 \, dr, \qquad \text{(Eq. 1)}$$

leads to a hyperbolic distribution of the blade chord over the blade radius for minimum power consumption. Parametric studies showed that also a trapezodial planform gives considerable performance improvements (Fig. 6)

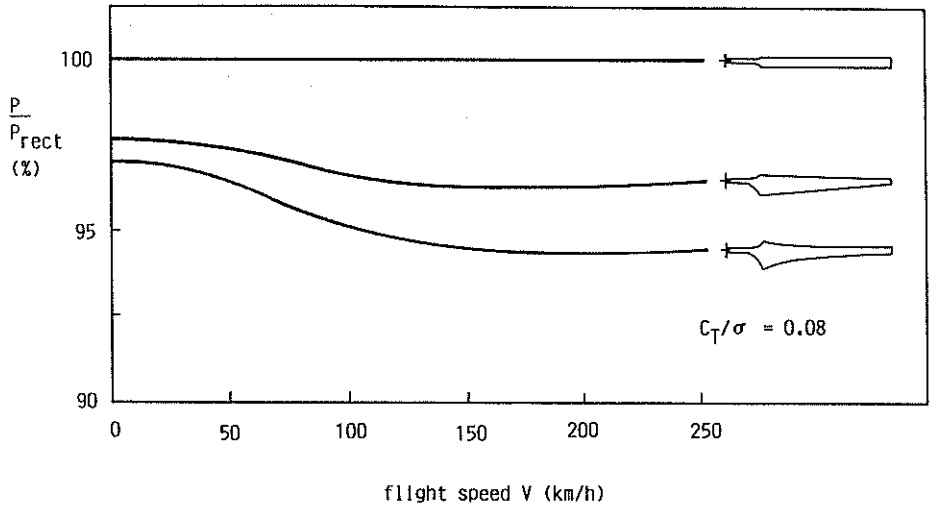

Fig. 6: Influence of blade tapering on rotor power consumption

Further benefits of a reduced blade chord in the tip region are obtained through the reduction of the vorticity in the blade tip region. This results in a reduced interaction of the tip vortex with the following blade and therefore in a reduction of induced power, vibration excitement and noise level.

To provide the same blade thrust

$$T = Z \cdot \frac{\rho}{2} \cdot \Omega^2 \cdot c_L \int_0^R c(r) \cdot r^2 \cdot dr \qquad \text{(Eq. 2)}$$

for a given average lift coefficient, a reduction of the blade chord due to the dynamic pressure distribution at the most effective outer blade parts requires an over-compensation of the lost blade area by an increased chord at the less effective inner blade parts and leads therefore to an increase of the blade weight.

From Eq. 2 follows, that the so-called "thrust-weighted" solidity s_T /10/ for different rotors of same thrust capability must be the same:

$$\sigma_T = \frac{3 \cdot Z}{\pi \cdot R^2} \int_0^R C(r) \cdot \left(\frac{r}{R}\right)^2 dR \qquad \text{(Eq. 3)}$$

Eq. 3 is derived for the hover condition, but model rotor wind tunnel tests /10/ have shown that it is roughly valid for forward flight too.

Similar effects as with blade tapering can be achieved by a high blade twist with the same favourable effects in power consumption and noise emission, due to the "smoother" lift distribution over the blade radius.

For integration of all these aerodynamic improvements new rotor blades, suitable for the BO105 with production bearingless rotor hub, were designed and built, see Fig. 7 and Table 2. The same blade area solidity of σ = .07 was applied as for the BO105 standard rotor. As a compromise between aerodynamic and weight considerations, a tapering to two-third of the inner blade chord was determined, beginning at 80 % blade radius, with rectangular inner blade part. The DM-H4 Tb was chosen for the retangular blade part, whereas the DM-H3 Tb was arranged at 98.5 % R with linear transition between the airfoils.
A new structural design was selected for the advanced rotor blades: A box type spar provides a higher torsional stiffness and gives the opportunity for aeroelastic tailoring, i.e. for nearly arbitrary positioning of the different elastic axes.

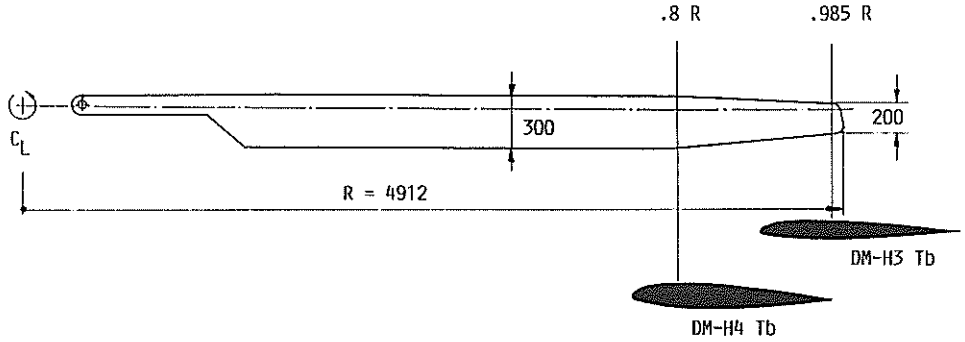

Fig. 7: Geometry of the advanced rotor blade

Intensive investigations were carried out for the determination of the optimum shape of the blade tip. In principle, a sweep back of the leading edge and a reduced airfoil thickness in the tip region will assure improvements in helicopter performance and a reduction of the unfavourable transonic effects at the advancing blade tip. Theoretical studies with a modern numerical method based on the solution of the Euler equations /5/ show a smooth local Mach number distribution over the tip for the new rotor blade (Fig. 8).

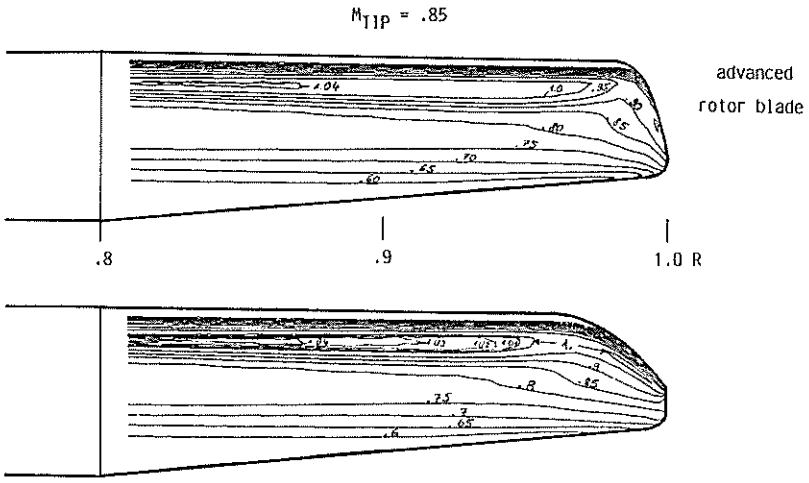

Fig. 8: Local Mach number on the upper surface of the advancing blade tip

4. Model Rotor Test

For verification of the predicted characteristics of the new rotor blade design a model rotor of 4 m diameter was built and tested in the 8 x 6 m test section of the Dutch German Wind Tunnel (DNW), s. Fig. 9. For comparison test data from a 4 m model rotor of the BO105 standard rotor were available.

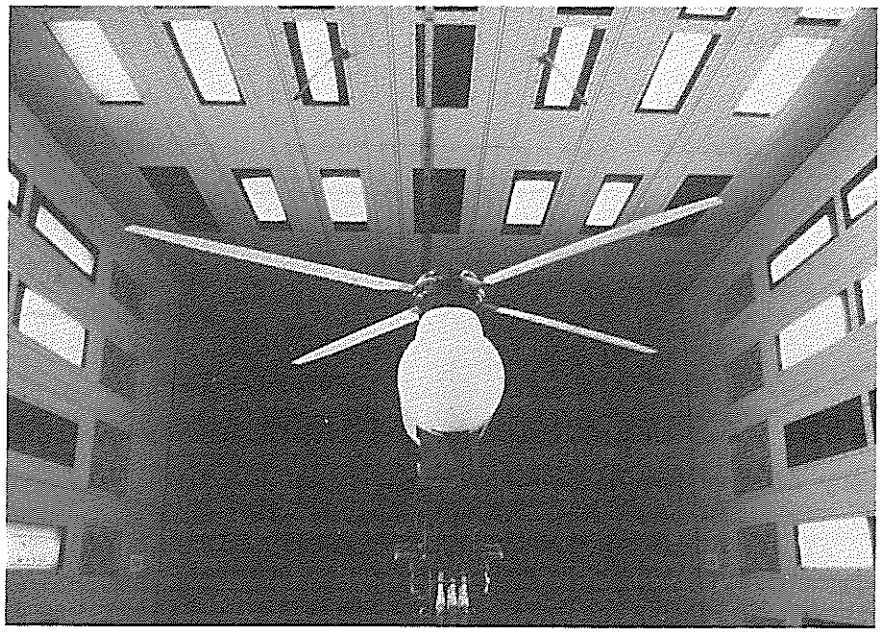

Fig. 9: Advanced model rotor in the DNW wind tunnel

Table 2 shows the characteristic data of the advanced model and full scale rotors in comparison with the corresponding BO105 standard rotor version.

	Advanced rotor		BO105 rotor	
	full scale	model	full scale	model
diameter (m)	9.84	4.0	9.82	4.0
number of blades	4	4	4	4
blade chord (m)	.30/.20[1)]	.135/.081[1)]	.27	.121
solidity	.07 [2)]	.0783 [2)]	.07	.077
blade twist (deg)	- 10		- 8	
blade airfoil	up to .8R: DM-H4 Tb at .985R : DM-H3 Tb		NACA 23012 mod.	
tip speed (m/s)	218	218	218	218

1) rectangular blade region/blade tip
2) thrust weighted solidity

Table 2: Characteristic data of the advanced rotor compared to the BO105 standard rotor (full scale and model)

During the wind tunnel tests blade load coefficients from .05 up to .12 were investigated under steady "flight" conditions at speeds up to 300 km/hr, corresponding to a maximum Mach number of .88 and an advance ratio of .39. Fig. 10 shows the range of operational conditions of the test campaign.

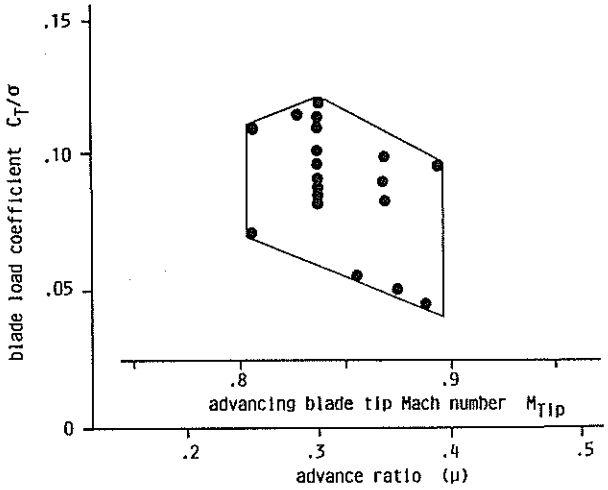

Fig. 10: Model rotor wind tunnel test operating conditions

A very smooth rotor behaviour was observed over the whole operation envelope. Compared to the standard BO105 model rotor performance improvements were in the predicted range except for hover. It was investigated outside the wind tunnel for inground-effect: instead of a 10 % power saving, as predicted, only 6 % were achieved . An explanation of this phenomenon was found later, during the whirl tower and flight tests (s. Chpt. 5 and 6).

In another test campaign the model rotor was used for intensive flowfield measurements with total pressure and hot wire probe sensors to get a better insight into the complicated nature of the rotor downwash /6/. Fig. 11 shows a typical result for the inplane component of the induced flowfield in transition flight.

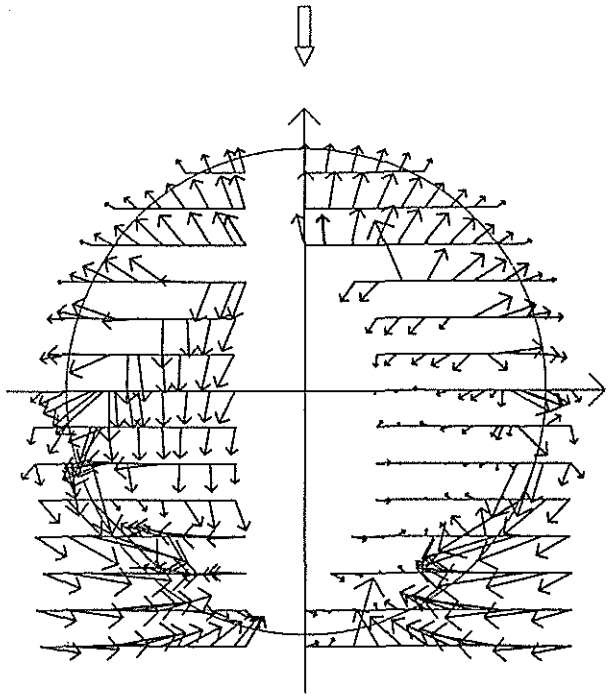

advanced model rotor

$\frac{z}{R} = .1$

$\mu = .06$

$C_T/\sigma = .073$

Fig. 11: Model rotor flowfield measurements.

5. Whirl Tower Tests

The full scale prototype rotor was tested on the MBB whirl tower at Ottobrunn. Similar performance results were obtained as during the model rotor tests: The predicted reduction in required power of about 10 % against the BO105 standard rotor was approximately achieved at low thrust values whereas at higher thrust the power saving was only 6 %.

It could be assumed that the induced power was higher than expected. A similar result was found in /8/, where the power saving due to the ground effect was reduced significantly with increasing blade twist.

The explanation for this phenomenon seems to be the low vorticity strengths of the not yet rolled-up tip vortices in the vicinity of the rotor disk, caused by the reduction of the lift at the outer blade parts with increasing blade taper and twist. This leads to less downwash contraction and therefore to a lower pressure level in the "air-cushion" between rotor and ground surface. This air cushion is the reason for the gain in required power at hover IGE. The reduction of this gain seems to be characteristic for modern high performance rotors.

6. Flight Tests

The prototype rotor was also flight tested on a BO105 LS, (Fig. 12), the most powerful version of the BO105 series /9/. The whole flight regime of the BO105 LS, including autorotation and dives with maximum tip Mach numbers up to .95 was covered in the tests.

Fig. 12: BO105 LS with advanced rotor blades

6.1 Performance

Hover performance was of particular interest because of the uncertaincies in the rig test results. In ground effect the same power saving of 6 % was measured (Fig. 13), whereas out of ground effect a reduction of 10 % was achieved as predicted (Fig. 14). The gain of 10 % was observed over the whole tested thrust range.

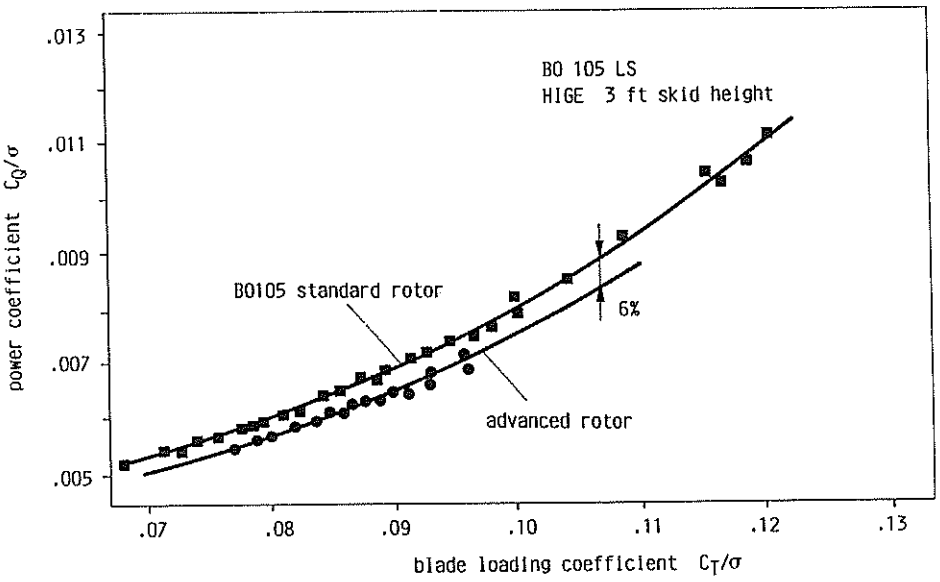

Fig. 13: Power consumption in hover flight IGE

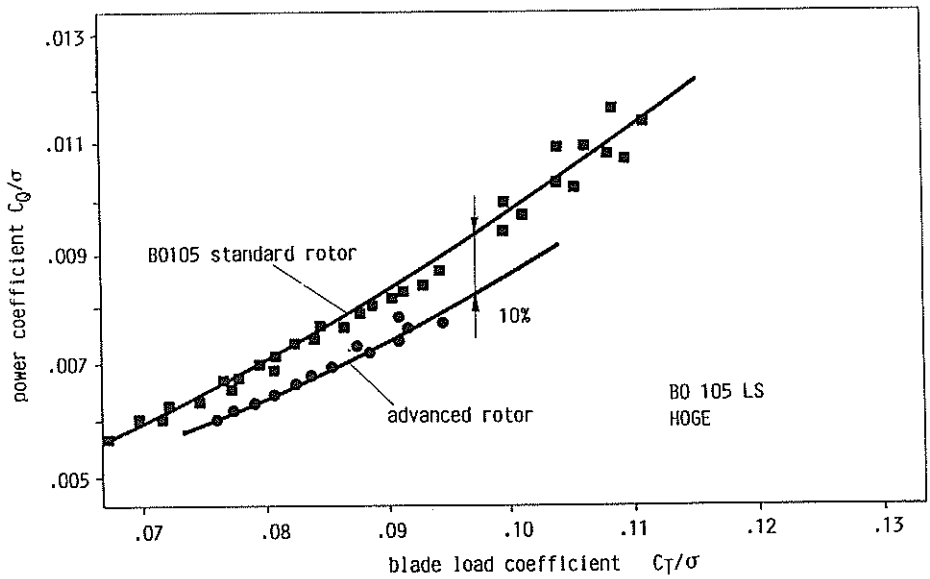

Fig. 14: Power consumption in hover flight OGE

Comparison of the maximal figure of merit for hover out of ground effect showed an improvement from .73 for the standard BO105 rotor to .78 for the advanced rotor (Fig. 15).

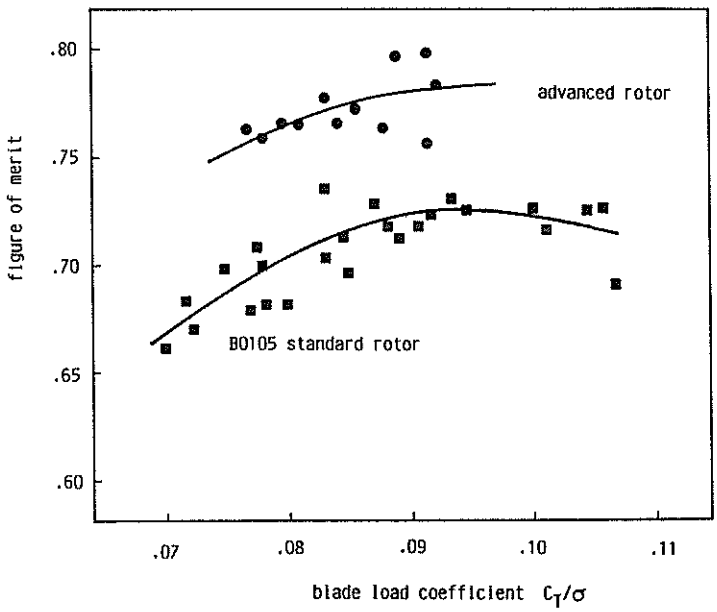

Fig. 15: Hover figure of merit

In forward flight the power consumption was also reduced significantly (Fig. 16). At higher advance ratios a reduction of about 10 % in total helicopter power required was achieved, leading to a higher maximum flight speed and a greater range of the helicopter. Fig. 16 shows the pure rotor profile power consumption. Profile power is the part of the total rotor power, which can be affected particularly by aerodynamic improvements of the blade.

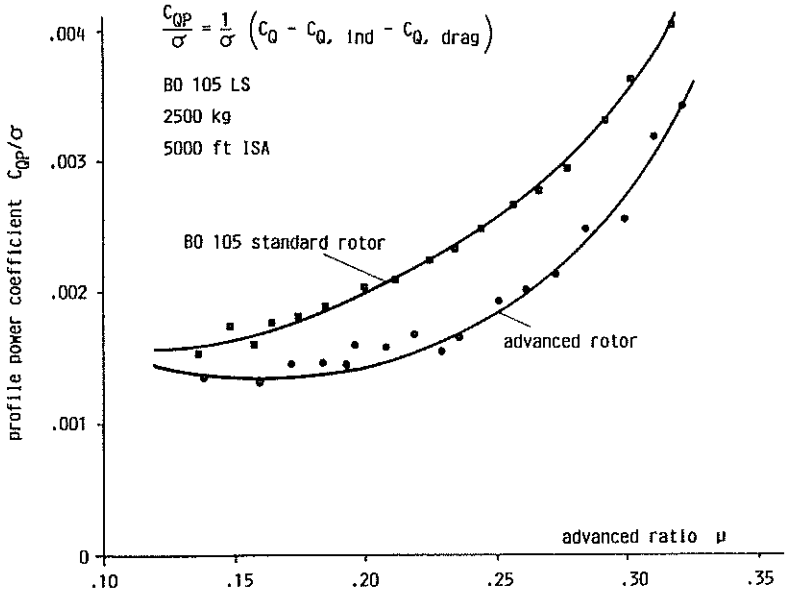

Fig. 16: Profile power consumption in forward flight

6.2 Flight Behaviour and Handling Qualities

6.2.1 Maximum Blade Loading

The maximum load factor was obtained from different flight manoeuvres. Normally, starting from a trimmed climb flight at a constant rate of climb of 1000 ft/min, turns were performed up to the maximum achievable load factor. The collective pitch was held constant during the manoeuvre. At higher speeds, where a rate of climb of 1000 ft/min could not be achieved because of exceeding the maximum continous power (MCP) limit, the flights were performed with MCP. The criteria for achieving the maximum load factor were the rotor stall and the blade load limits, especially the pitch link load. During the flight tests the permitted loads were observed continually.

As the maximum achievable load factor depends on the collective pitch level, flight tests with variing power settings were conducted, too. By starting the manoeuvre from a level or descent flight, the pitch link loads were significantly lower at the same load factor as compared to manoeuvres starting from climb flight. This means that at lower collective pitch the rotor stall occurs at higher load factors. During the latter manoeuvre type extreme rates of descent of up to 6000 ft/min occured. Therefore most of the flight tests were started with a rate at climb of 1000 ft/min or with MCP.

For comparing the test results of different flight conditions the blade loading coefficient

$$C_{T/\sigma} = \frac{n_z \cdot m \cdot g}{\rho \cdot (\Omega \cdot R)^2 \cdot z \cdot c \cdot R} \qquad \text{(Eq. 4)}$$

is plotted versus the advance ratio m. The formula for $C_{T/s}$ assumes a constant blade chord length over the radius. For the tapered DM-blades the equivalent blade area solidity (Chapt. 3) is applied.

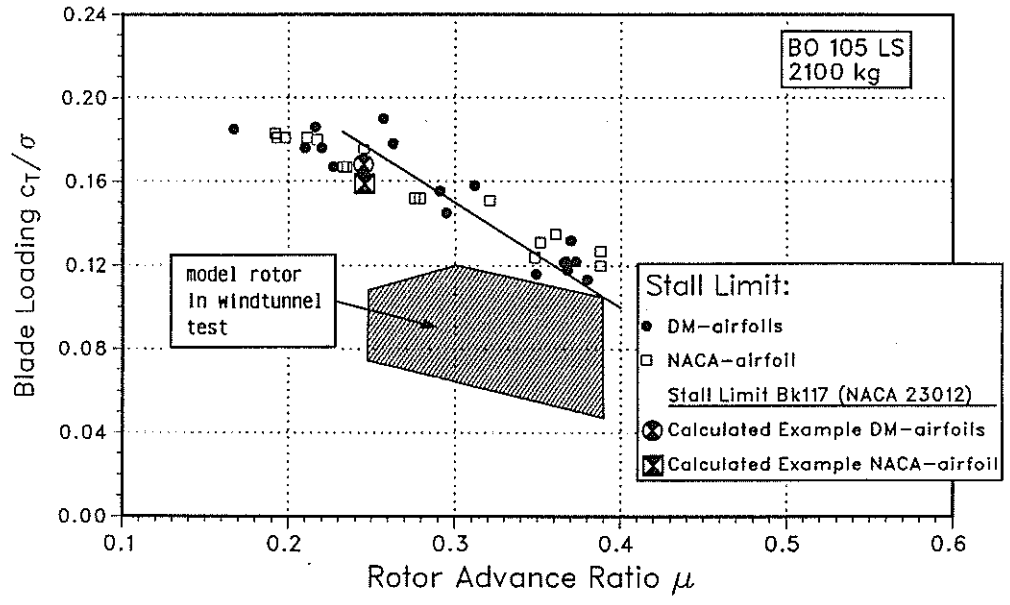

Figure 17: Maximal blade loading versus advance ratio

Fig. 17 shows the flight test results for the maximum achievable blade loading. With the advanced rotor blades the same high blade loading coefficients are achieved as with the BO105 standard rotor. The stall limit of the BK117, as determined from former flight tests, was slightly exceeded. Also plotted in Fig. 17 are the blade loads of the wind tunnel tests, showing generally lower blade loading because of the steady operational conditions.

A theoretical simulation of a turn near the stall limit requires an appropriate modelling of the unsteady aerodynamic behaviour of the airfoils in the stall region. The calculation results showed at the same advance ratio a higher blade loading for the DM-airfoils. In Fig. 17 calculation points of a turn with the maximum achievable load factor at 200 km/hr are presented. The normalized points are adequate for load factors 2.2 g for the advanced rotor blades and 2.1 g with the standard BO105 rotor, both for a gross mass of 2100 kg.

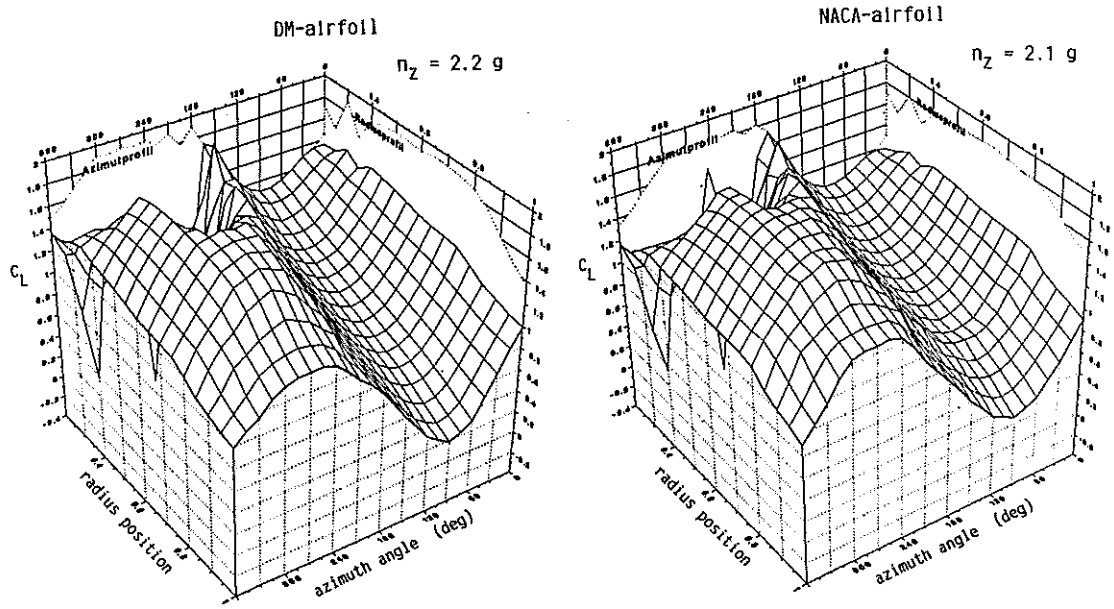

Fig. 18: Blade lift coefficients (BO105 LS, left turn with 200 km/hr)

Fig. 18 showes the variation of the lift coefficient over azimuth angle and radius for these two cases. The higher achievable maximum lift coefficient of the DM-H4 Tb airfoils is recognizable at the retreating blade between 40 % and 80 % radius.

6.2.2 Longitudinal stability

In the FAR Part 27 requirements for the static longitudinal stability of a helicopter a clear correlation between longitudinal stick position and flight speed is demanded: A forward shift of the control stick must cause a speed increase and vice versa. For compliance the stick position has to be varied from .7 to 1.1 VH, starting from a trimmed level flight while the collective pitch is to be held constant.

For conventional helicopter configurations there is a direct relationship between the pitching moment of the main rotor and the flight speed. Static instability can occur, if, together with the nose down moment due to the control input, the rotor produces an additional nose down moment with increasing flight speed. This negative speed stability determines the static stability: A more negative speed stability causes a deterioration of the static stability and vice versa.

The pitching moment coefficient C_M of the rotor blade airfoil is of particular influence on the main rotor speed stability. In forward flight an airfoil with negative C_M causes at the advancing blade tip, which dominates in the airload and therefore determines the behavior of the complete rotor, an increasing nose down moment with increasing flight speed. This means negative speed stability of the rotor.

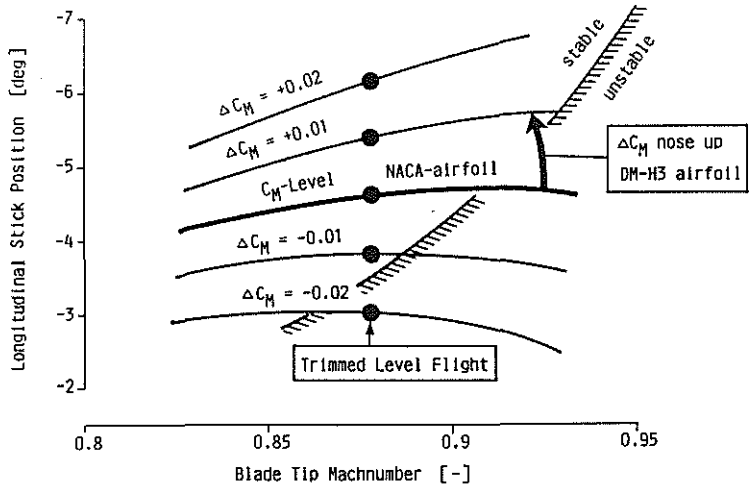

Fig. 19: Influence of different C_M-levels on static longitudinal stability

Fig. 19 shows the direct influence of different C_M-levels on the static stability: Stable behavior is provided up to a certain Mach number, which depends on the C_M-level of the blade airfoil. The blade tip Mach number in Fig. 19 is equivalent to the helicopter cruising speed including the influence of OAT and rotor tip speed. The reference line in Fig. 19 is determined for the NACA 23012 airfoil. For the generation of the different curves, only the C_M-level was varied. The positive effect of a more nose-up airfoil pitching moment is evident.

For the DM-H3 Tb airfoil the C_M-offset, compared to the NACA 23012, is nearly constant and of the order of magnitude of .01 (see Fig.4). However, a more positive C_M-value than realized for the DM-H3 Tb would be unfavorable due to higher drag and thereby higher power consumption and because of load aspects.

A further improvement of the static stability of the rotor results from a higher Mach number boundary for the Mach tuck (Chpt. 2) of the DM-H3 Tb airfoils.The higher Mach tuck boundary causes a smaller nose down pitching moment increase with increasing Mach number and therefore less negative speed stability of the rotor.

For the flight test program of the BO105 LS the most critical conditions for static stability, such as low gross weight, high air density and forward C.G. position, were considered. Thereby the influence of stall effects on the retreating blade, requiring a more forward stick position and simulating an apparent improvement of the longitudinal stability, could be eliminated.

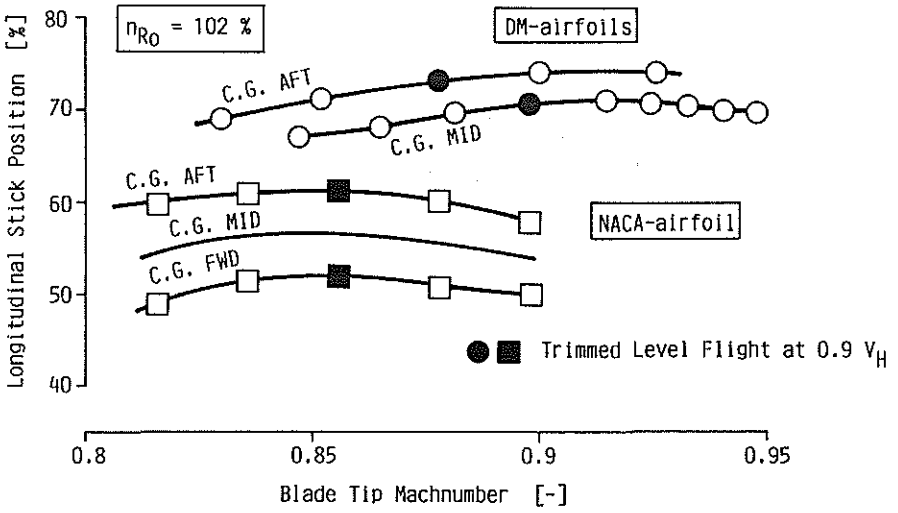

Fig. 20: Experimental results for the static longitudinal stability

Fig. 20 shows the longitudinal stick position versus blade tip Mach number for the BO105 LS standard rotor with NACA 23012 airfoil and the advanced rotor with DM-airfoils. Under extreme conditions, namely high rotor tip speed (102 %) and low OAT, a blade tip Mach number of .95 was reached with the new rotor. The improvement in static stability due to the advanced rotor blates is significant.

Beside the aerodynamic effects, the smooth transition from stable to unstable behavior of the rotor is also caused by the greater torsional stiffness of the DM blades. In this case the nose down pitching moment of the blade airfoils at high Mach numbers causes a smaller elastic blade twist, which results in a more stable stick position, compared to the standard BO105 rotor.

6.3 Vibrations and noise emission

The vibration level of the BO105 LS was significantly reduced with the advanced rotor blates due to the new airfoils and the dynamic characteristics of the blades. Fig. 21 shows that at the pilot seat a nearly 50 % reduction of the 4/rev vertical acceleration was measured for flight speeds greater than 90 km/hr.

Theoretical investigations showed a reduction in noise emission by about one PNdB, especially due to the reduced blade chord at the tip regionregion. Accurate data will be obtained from future noise measurements.

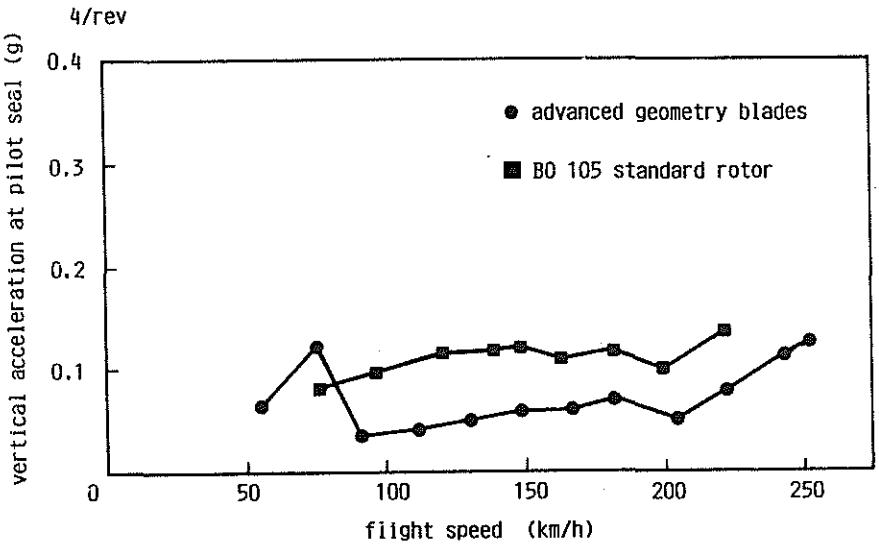

Fig. 21: BO105 LS cabin vibration level

7. Conclusions

A new helicopter rotor blade was developed at MBB using advanced aerodynamic and structural technology. New airfoils, a tapered outer blade region and a specific tip geometry were integrated in the new blade design. A prototype rotor was built and tested in model and full scale versions.

Predicted performance improvements were verified in flight tests. In comparison to the BO105 standard rotor a 10 % reduction in power consumption was achieved for hover OGE and for forward flight. At hover IGE a 6 % reduction was found, due to the smaller ground effect gain of high performance rotors.

A slight increase of maximum thrust capability was obtained at the same equivalent blade area solidity. The longitudinal stability is significantly improved due to the airfoil characteristics and the higher torsional stiffness of the blades. Also considerable reduction of the vibration level was achieved.

The new aerodynamic blade technology will be applied for MBB's future civil and military helicopter generation.

8. References

/1/ H. Huber, A. Teleki, C. Schick — Hochgeschwindigkeitserprobung des Hubschraubers BO105 HGH, Ninth DGLR Annual Symposium, Munich 1975

/2/ H. Huber — Helicopter flight characteristics improvement through swept tip rotor blades, Fivth European Rotorcraft Forum, Amsterdam 1979

/3/ K.H. Horstmann, H. Köster, G. Polz
Development of new airfoil sections for helicopter rotor blades
Eigth European Rotorcraft Forum, Aix-en-Provence 1982, Paper No. 2.2

/4/ K.H. Horstmann, H. Köster, G. Polz
Improvement of two airfoil sections for helicopter rotors
Tenth European Rotorcraft Forum, The Hague 1984, Paper No. 1

/5/ H. Stahl
Application of 3D Euler code to transonic blade tip flow
Twelfth European Rotorcraft Forum, Garmisch 1986, Paper No. 29

/6/ B. Junker, W. Gradl, V. Mikulla
Model rotor wake measurements in a wind tunnel
13th European Rotorcraft Forum, Arles 1987

/7/ L. Dadone
Rotor airfoil optimization: An understanding of the physical limits
34th Annual Forum of the American Helicopter Society, Washington 1978

/8/ D.T. Balch
Experimental study of main rotor/tail rotor/airframe interaction in hover
39th Annual Forum of the American Helicopter Society, St. Louis 1983

/9/ A. Horlebein, G. Polz
Development of the BO105 LS
32nd Annual Meeting of the Canadian Aeronautics and Space Institute Montreal 1985

/10/ M.A. Mc Veigh, F.J. Mc Hugh
Recent advances in rotor technology at Boeing Vertol
38th Annual Forum of the American Helicopter Society, Anaheim 1982